Journal of Hazardous Materials 433 (2022) 128716

Contents lists available at ScienceDirect

Journal of Hazardous Materials

journal homepage: www.elsevier.com/locate/jhazmat

Sulfate-accelerated photochemical oxidation of arsenopyrite in acidic systems under oxic conditions: Formation and function of schwertmannite

Jun Hong [a,b], Lihu Liu [b], Ziwei Zhang [b], Xiange Xia [a,*], Li Yang [a], Zengping Ning [c], Chengshuai Liu [c], Guohong Qiu [b,*]

[a] Key Laboratory of Fertilization from Agricultural Wastes, Ministry of Agriculture and Rural Affairs, Institute of Plant Protection and Soil Fertilizer, Hubei Academy of Agricultural Sciences, Wuhan 430070, Hubei Province, China
[b] College of Resources and Environment, Interdisciplinary Sciences Institute, Huazhong Agricultural University, Wuhan 430070, Hubei Province, China
[c] State Key Laboratory of Environmental Geochemistry, Institute of Geochemistry, Chinese Academy of Sciences, Guiyang 550081, Guizhou Province, China

HIGHLIGHTS

- SO_4^{2-} accelerates the photochemical oxidation of arsenopyrite.
- Fe(II) released from arsenopyrite is oxidized by ROS to form schwertmannite.
- LMCT in schwertmannite–As(III) contributes to arsenopyrite and As(III) oxidation.
- Photooxidation rate of arsenopyrite increases with increasing pH from 2.0 to 4.0.

GRAPHICAL ABSTRACT

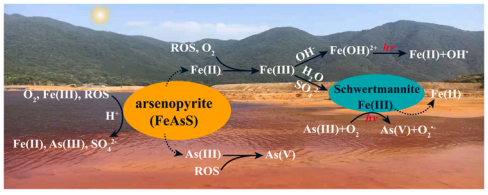

ARTICLE INFO

Editor: Prof. Dr. Yang Deng

Keywords:
Arsenopyrite
Photochemical oxidation
Acid mine drainage
Sulfate
Schwertmannite

ABSTRACT

The weathering of arsenopyrite is closely related to the generation of acid mine drainage (AMD) and arsenic (As) pollution. Solar radiation can accelerate arsenopyrite oxidation, but little is known about the further effect of SO_4^{2-} on the photochemical process. Here, the photooxidation of arsenopyrite was investigated in the presence of SO_4^{2-} in simulated AMD environments, and the effects of SO_4^{2-} concentration, pH and dissolved oxygen on arsenopyrite oxidation were studied as well. SO_4^{2-} could accelerate the photooxidation of arsenopyrite and As (III) through complexation between nascent schwertmannite and As(III). Fe(II) released from arsenopyrite was oxidized to form schwertmannite in the presence of SO_4^{2-}, and the photooxidation of arsenopyrite occurred through the ligand-to-metal charge-transfer process in schwertmannite–As(III) complex along with the formation of reactive oxygen species in the presence of O_2. The photooxidation rate of arsenopyrite first rose and then fell with increasing SO_4^{2-} concentration. In the pH range of 2.0–4.0, the photooxidation rate of arsenopyrite progressively increased in the presence of SO_4^{2-}. This study reveals how SO_4^{2-} promotes the photooxidation of arsenopyrite and As release in the AMD environment, and improves the understanding of the transformation and migration of As in mining areas.

1. Introduction

The demand for mineral resources is growing with the socioeconomic development (Tabelin et al., 2020a). For example, in order to satisfy the needs for key metals such as copper, gold, zinc, nickel, and cobalt in the fields of computers, aviation, electric vehicles,

* Corresponding authors.
E-mail addresses: 13607123150@139.com (X. Xia), qiugh@mail.hzau.edu.cn (G. Qiu).

https://doi.org/10.1016/j.jhazmat.2022.128716
Received 8 January 2022; Received in revised form 12 March 2022; Accepted 13 March 2022
Available online 17 March 2022

and clean/renewable energy, sulfide deposits containing these metals are continuously mined (Aikawa et al., 2020; Nansai et al., 2014). The chemical and biological oxidation of sulfide minerals frequently occurs in wastes and leads to the generation of acid mine drainage (AMD) (Aikawa et al., 2020; Thao et al., 2020; Tomiyama et al., 2020). Due to its low pH and heavy metal pollution, AMD poses serious threats to waters, soils and biology around the mining and downstream areas (Gray, 1998). Notably, AMD also affects the weathering of sulfide minerals and intensifies environmental pollution (Cheng et al., 2009; Tabelin et al., 2020b). Sulfide minerals mainly include pyrite, chalcopyrite, pyrrhotite, galena and arsenopyrite (Rodríguez-Galán et al., 2019). As one of the most common arsenic-containing iron sulfide minerals, arsenopyrite is often found in auriferous sulfide ores, and its oxidative dissolution can cause serious arsenic (As) pollution (Murciego et al., 2011; Park et al., 2021). As pollution has caused serious human health problems and environmental challenges in the world. Humans are usually exposed to As through drinking water and food chain. When large amounts of As-containing compounds are ingested, acute As poisoning occurs and usually results in multiple organ failure and death, whereas prolonged exposure to As at very low concentrations will also lead to chronic As poisoning (Bagchi, 2007; Tabelin et al., 2018). Globally, more than 150 million people suffer from the risk of As contamination in drinking water (Singh et al., 2015). Therefore, dissection of the oxidative dissolution process of arsenopyrite will improve the understanding of AMD and reduce the risk of As pollution for humans.

In the AMD environment, SO_4^{2-} and Fe^{3+}/Fe^{2+} ions are the main anions and cations, respectively (Cheng et al., 2009; Rodríguez-Galán et al., 2019). Fe^{3+}/Fe^{2+} can transfer electrons in redox reaction and directly participates in the weathering of iron sulfide minerals (Kaplun et al., 2011; Mazumdar et al., 2008; Neil and Jun, 2016). In this process, iron (hydr)oxides will be formed, which have high adsorption capacities for anionic heavy metals such as As(III,V) and Cr(III,VI) and affect the geochemical behavior of heavy metals in waters and soils (Cheng et al., 2009; Yang et al., 2019). Therefore, the oxidation process of arsenopyrite mediated by Fe^{3+}/Fe^{2+} has attracted great research attention and concerns (Neil and Jun, 2016; Yunmei et al., 2004). Common inorganic anions usually affect the oxidative dissolution of arsenopyrite and the corresponding release of As. As previously reported, although Cl^- is not directly involved in the redox reaction of arsenopyrite, it can penetrate the elemental S^0 passivation film formed on arsenopyrite and promote its oxidative dissolution (Zheng et al., 2020). The effects of anions on the oxidation rate of arsenopyrite follow the order of $SO_4^{2-} < Cl^- < NO_3^-$ in acidic solutions, which may be attributed to the effect of anions on the release rate of Fe and As from arsenopyrite (Mikhlin et al., 2006). Phosphate can promote the oxidation of arsenopyrite and release of As through complexation on the mineral surface in near-neutral pH environments (Wu et al., 2020). In addition, some studies have revealed that the presence of phosphate may also lead to the formation of $FePO_4$ coating on the arsenopyrite surface, which inhibits the further oxidation of arsenopyrite (Park et al., 2021). SO_4^{2-} is the most common and abundant inorganic anion in the AMD environment. However, much less attention has been paid to the influence of SO_4^{2-} on the oxidation process of arsenopyrite in current research.

Field survey results have suggested that the concentrations of many metals including As, Zn and Mn exhibit diurnal cycle changes in mountain streams or mine drainage (Nimick et al., 2003, 2011; Sarmiento et al., 2007), which is likely associated with the oxidative dissolution of metal minerals under solar radiation (Hong et al., 2018, 2020). In the earth's surface environment exposed to solar radiation, inorganic anions also participate in the migration and transformation of metal elements with the formation of reactive oxygen species (ROS) in photochemical reactions under solar radiation. Our previous studies have shown that $FeOH^{2+}$ facilitates the generation of ROS including $^{\bullet}OH$ and H_2O_2 and promotes the release of As from arsenopyrite due to the photo-Fenton reaction under near-UV radiation (Hong et al., 2018). ROS including $^{\bullet}OH$ and $O_2^{\bullet-}$ are formed when NO_3^- is excited by UV radiation, which will promote the oxidation of Mn(II) to manganese oxides (Chu and Anastasio, 2003; Mack and Bolton, 1999; Zhang et al., 2018a). $Cl^{\bullet}$ and $SO_4^{\bullet-}$ can be respectively formed when $FeCl^{2+}$ and $FeSO_4^+$ are exposed to near-UV radiation and acidic conditions (Emett and Khoe, 2001; Machulek et al., 2009). However, the effect and mechanism of SO_4^{2-} on As release from arsenopyrite in photochemical reaction remain to be elucidated.

In the oxygen-rich AMD environment, weakly crystallized iron (hydr)oxides, namely schwertmannite ($Fe_8O_8(OH)_{8-2x}(SO_4)_x$; $1 < x < 1.75$), can be formed in the presence of SO_4^{2-} and Fe(III) with chloride at low concentrations (Igarashi et al., 2020; Liu et al., 2018; Paikaray et al., 2011). Schwertmannite not only displays high adsorption capacities for anionic heavy metals (As and Cr) (Burton et al., 2009; Regenspurg and Peiffer, 2005), but also has certain photochemical reactivity. Under exposure to UV radiation, electron transfer occurs between Fe(III) and citric acid/oxalate on the schwertmannite surface, which can promote the photochemical reductive dissolution of schwertmannite with the formation of ROS in acidic solutions (Guo et al., 2015; Wu et al., 2012). The oxidative dissolution of minerals containing heavy metals through galvanic interactions may be an important factor for environmental pollution in mining areas (Liu et al., 2008). As(III) and Sb(III) complex with ferrihydrite, and are then respectively oxidized to As(V) and Sb(V) through a ligand-to-metal charge-transfer (LMCT) process along with the generation of $O_2^{\bullet-}$ in the presence of O_2 under UV radiation (Kong et al., 2016; Xu et al., 2014). SO_4^{2-} may react with the released iron ions to form schwertmannite, which further affects the oxidation of arsenopyrite and dissolved As(III) through photochemical reactions under solar radiation in the AMD environment.

Mg^{2+} is commonly detected in AMD at high concentrations (5–69 mmol L^{-1}) (Heviánková et al., 2014; Rodríguez-Galán et al., 2019). In this work, $MgSO_4$ was selected to investigate the oxidative dissolution mechanism of arsenopyrite in the presence of SO_4^{2-} under UV radiation, and the effects of initial SO_4^{2-} concentration, pH and dissolved oxygen on the oxidation process were further studied. The findings are expected to provide some new theoretical guidance for environmental control of As pollution in mining areas.

2. Materials and methods

2.1. Reagents and materials

The natural arsenopyrite used in this work was collected from Hechi, Guangxi Zhuang Autonomous Region, China. The main components (FeAsS) and surface properties of the minerals were determined by powder X-ray diffraction (XRD, Shimadzu 6100) and Fourier transform infrared (FTIR, Bruker VERTEX 70), respectively (Fig. S1a, b). The details of pretreatment process of minerals are presented in supporting information SI. $MgSO_4$ (AR), Na_2SO_4 (AR), $MgCl_2$ (AR), H_2SO_4 (AR), HCl (AR), tert-butyl alcohol (TBA, $\geq$ 99.0%), benzoic acid (BA, $>$ 99.5%) and *p*-hydroxybenzoic acid (*p*-HBA, $\geq$ 99.0%) were purchased from Sinopharm Chemical Co., Ltd.

2.2. Photooxidation of arsenopyrite in the presence of $MgSO_4$

Fig. S2a shows the reaction device for the photochemical experiments. There is a 220 mm $\times$ 185 mm LED-UV lamp with 30 W power on the back and left side of the 500 mL quartz five-mouth bottle, respectively, and a magnetic stirrer is placed beneath the quartz bottle. The UV radiation that reaches the Earth's surface is mainly UV-A (315–400 nm), and the light intensity increases with increasing wavelength. The main wavelength of the selected LED-UV lamp was 395 nm to simulate the sunlight radiation (Fig. S2b) (Kerr and Fioletov, 2008). The light intensity was 20.0 mW cm^{-2} at 375–475 nm (λ_{peak} = 420 nm) as determined by a UV-A radiation meter. In the dark reaction experiment, the quartz bottle was wrapped by tinfoil with the LED-UV lamp

disconnected from the power supply.

The quartz bottle was open to air so as to provide an aerobic reaction environment. The oxygen content was measured to be about 8.5 mg L^{-1} in the reaction solution. About 0.15 g arsenopyrite and 300 mL $MgSO_4$ solution at 0–10 mmol L^{-1} were added to the quartz bottle, and the initial pH of the suspension was adjusted to 2.0–4.0 using 0.025–0.25 mol L^{-1} H_2SO_4. During the reaction, the fluctuation of the pH value in the suspension was less than 0.03, 0.03 and 0.2 at pH 2.0, 3.0 and 4.0, respectively. To further investigate the effect of dissolved oxygen on the photooxidation of arsenopyrite in the presence of $MgSO_4$, high-purity nitrogen (99.999%) was first continuously passed through the solution without arsenopyrite for more than 30 min, and then the suspension was kept under nitrogen flow during the whole reaction. The oxygen content was measured to be below 0.1 mg L^{-1} in the reaction solution. Aliquots (20 mL) of the suspension were taken out at different time, and then solid-liquid separation was performed by using microporous membrane.

To explore the effect of ROS intermediate on the photooxidation of arsenopyrite in the presence of $MgSO_4$, 0.1 mol L^{-1} TBA was added to the reaction system as an $^{\bullet}OH$ scavenger (Ryu et al., 2013). BA can capture $^{\bullet}OH$ and then be converted to more stable *p*-HBA (Zhang et al., 2016a). 10.0 mmol L^{-1} BA was added for further quantitative detection of $^{\bullet}OH$ concentration. To clarify the possible influencing mechanism of SO_4^{2-} on the photochemical reaction process, 0.15 g arsenopyrite and 300 mL of $MgCl_2$ solution (at 0 and 2.5 mmol L^{-1}) were added to the quartz bottle, and the initial pH of the suspension was adjusted to 4.0 with 0.05–0.5 mol L^{-1} HCl. All the above experiments were repeated three times to ensure the accuracy of the experimental data.

2.3. Analysis methods

The concentrations of total Fe (Fe(T)) and Fe(II) were analyzed using the 1, 10-phenanthroline analytical method at 510 nm (Qiu et al., 2016). The concentrations of total As (As(T)) and As(III) were measured by a hydride generation-atomic fluorescence spectrometer (Xu et al., 2014). The detection limit and relative standard deviation (RSD) of the 1, 10-phenanthroline analytical method and hydride generation-atomic fluorescence spectrometer are presented in the supporting information SII. The concentration of H_2O_2 was determined by *N*, *N*-diethyl-*p*-phenylenediamine spectrophotometry at 551 nm (Lee and Choi, 2002). The concentration of *p*-HBA was quantified by high performance liquid chromatography (HPLC) at 255 nm, and the concentration of $^{\bullet}OH$ was about 6 times that of *p*-HBA (Zhang et al., 2018a). Qualitative analysis of $^{\bullet}OH$, $SO_4^{\bullet-}$ and $O_2^{\bullet-}$ was performed by electron paramagnetic resonance spectrometer (EPR, Bruker EMX-PLUS) using 5, 5-dimethyl-1-pyrroline N-oxide (DMPO, 100 mmol L^{-1}) as spin trapping agents. The crystal structure changes and surface properties of the arsenopyrite before and after the reaction were characterized by XRD, FTIR, scanning electron microscope (SEM, Hitachi SU8000) and X-ray absorption fine structure (XAFS, Beijing Synchrotron Radiation Facility, 1W1B beamline). The detailed analysis process of XAFS is presented in the supporting information SII.

The speciation of Fe(III) is affected by pH, concentration and coexisting anions in the solution. In order to determine the speciation of dissolved Fe(III) with various coexisting anions at different pH values, the chemical speciation distribution of Fe(III) was calculated and analyzed with the HYDRA/MEDUSA software (Zhou et al., 2014).

3. Results

3.1. Photooxidation of arsenopyrite in the presence of SO_4^{2-}

Fig. 1 shows the concentrations of As and Fe species in the systems of single arsenopyrite and a mixture of arsenopyrite and 5.0 mmol L^{-1} $MgSO_4$ in air atmosphere at pH 3.0 under UV radiation. In the single arsenopyrite suspension, the concentrations of As(III,V) and Fe(II) continuously increased with reaction time, and the As(T) and Fe(II) concentrations respectively reached 62.0 and 67.3 μmol L^{-1} after 6 h (Fig. 1c, d). The concentration of Fe(III) first increased and then decreased, and finally tended to equilibrium with time, and the maximum concentration approached to 6.1 μmol L^{-1} (Fig. 1d). In the

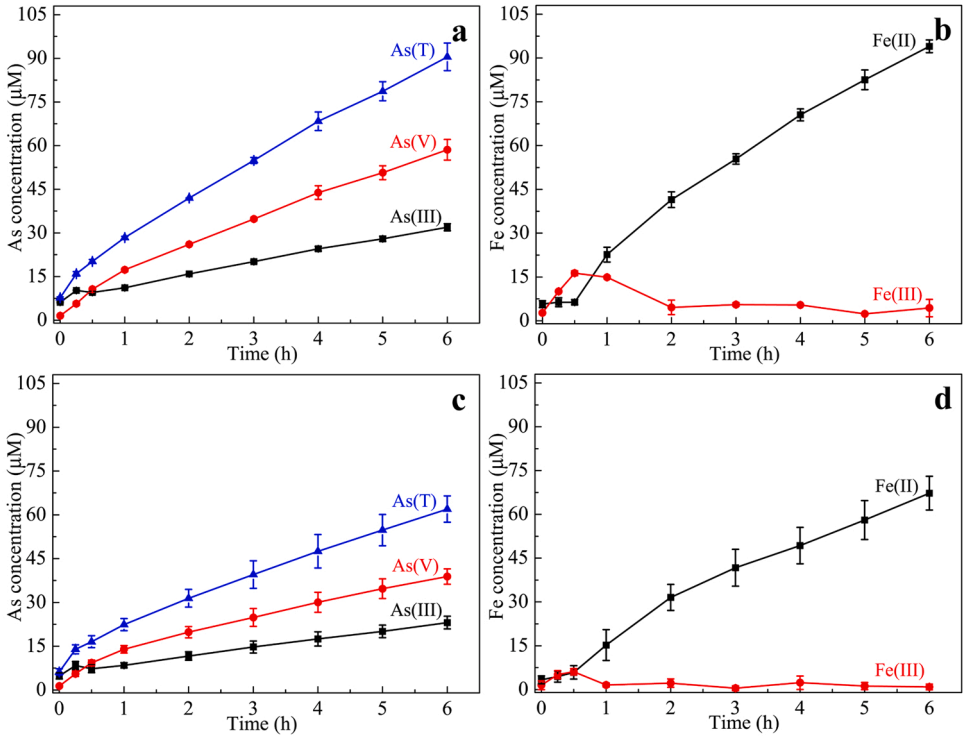

Fig. 1. Concentrations of dissolved As and Fe species in the mixed system of arsenopyrite (0.5 g L^{-1}) and $MgSO_4$ (5.0 mmol L^{-1}) (a, b), and in the single arsenopyrite (0.5 g L^{-1}) system (c, d) under UV radiation at pH 3.0 in air atmosphere.

mixed suspension of arsenopyrite and $MgSO_4$, a similar changing trend of As(III,V) and Fe(II,III) concentrations was observed. The concentration of As(T) and Fe(II) respectively increased to 90.5 and 94.0 μmol L^{-1} after 6 h, and the maximum Fe(III) concentration reached 16.3 μmol L^{-1} (Fig. 1a, b). The above results suggested that $MgSO_4$ could accelerate the photooxidation of arsenopyrite under UV radiation. To further confirm this phenomenon, the oxidation of arsenopyrite was conducted under dark conditions at pH 3.0 in air atmosphere (Fig. S3). Dissolved Fe(III) was not detected in the two systems; and the concentration of As(III,V) and Fe(II) showed a similar changing trend to that under UV radiation. The As(T) and Fe(II) concentration reached 43.8 and 44.5 μmol L^{-1} at 6 h in the mixed system of arsenopyrite and 5.0 mmol L^{-1} $MgSO_4$ (Fig. S3a, b), which were not obviously different from those in the single arsenopyrite suspension (41.0 and 43.8 μmol L^{-1}, respectively) under dark conditions (Fig. S3c, d). These results further confirmed that $MgSO_4$ could promote the photooxidation of arsenopyrite under UV radiation.

The solid products generated in the mixed system of arsenopyrite and $MgSO_4$ at 6 h were further characterized under UV radiation and dark conditions. Fig. 2a shows the XRD patterns of the solid products, and no obvious change was observed for the crystal structure of arsenopyrite. In the FTIR spectra, the absorption band at 431 cm^{-1} is attributed to the S_2(–II) stretching vibration in arsenopyrite (Wang et al., 2021). The absorption bands at 1636 and 3425 cm^{-1} are respectively attributed to H–O–H bending vibration and O–H stretching vibration of H_2O (Zhang and Yuan, 2017). The absorption bands at 601, 658, 1068, 1123 and 1174 cm^{-1} are due to S–O vibration of SO_4^{2-} (Borda et al., 2004; Tabelin et al., 2017a; b). No obvious change was observed in the FTIR spectra and micromorphology of arsenopyrite before and after reaction under UV radiation (Figs. S1b, 2b and S4).

The effect of $MgSO_4$ concentration on the photooxidation of arsenopyrite was studied at pH 3.0 in air atmosphere (Figs. 3 and S5). The changing trend of As and Fe species concentration in the mixed systems with $MgSO_4$ (1.0–10.0 mmol L^{-1}) over time was consistent with that in the single arsenopyrite system (Figs. 1, 3, S3 and S5). At 1.0, 5.0 and 10.0 mmol L^{-1} $MgSO_4$, the final concentrations of As(T) and Fe(II) were respectively 77.3 and 80.4 μmol L^{-1}, 90.5 and 94.0 μmol L^{-1}, 79.4 and 84.1 μmol L^{-1} under UV radiation (Figs. 1 and 3), and 41.3 and 45.1 μmol L^{-1}, 43.8 and 44.5 μmol L^{-1}, 41.1 and 44.9 μmol L^{-1} under dark conditions (Figs. S3 and S5). The above results indicated that $MgSO_4$ at 0–10.0 mmol L^{-1} has no obvious effect on the oxidation of arsenopyrite under dark conditions, but could significantly enhance the photooxidation rate of arsenopyrite under UV radiation.

Our previous results have shown that ROS are formed to affect the oxidation of arsenopyrite under UV radiation (Hong et al., 2018). The addition of TBA decreased the concentrations of As(T) and Fe(T) by 13.0% and 27.0%, respectively, in the mixed system of arsenopyrite and 5.0 mmol L^{-1} $MgSO_4$ under UV radiation (Fig. 4a, b). The cumulative $^{\bullet}OH$ concentration increased with reaction time, and the instant H_2O_2 concentration first rose and reached the maximum at 1 h, and then fell and finally tended to equilibrium with time (Fig. 4c). The EPR spectra further revealed that $^{\bullet}OH$, $SO_4^{\bullet-}$ and $O_2^{\bullet-}$ were formed in the mixed system under UV radiation, and relative intensity of the peaks of $^{\bullet}OH$ and $O_2^{\bullet-}$ was significantly higher than that of $SO_4^{\bullet-}$ (Fig. 4d) (Wei et al., 2017; Yu et al., 2020; Zhang et al., 2018b). These results indicated that ROS including $^{\bullet}OH$, H_2O_2, $O_2^{\bullet-}$ and $SO_4^{\bullet-}$ are the intermediates in the reaction system under UV radiation, which may affect the oxidation process of arsenopyrite.

3.2. Effects of pH and dissolved oxygen

The pH of AMD usually ranges from 2.0 to 4.0, and arsenopyrite oxidation experiments were further conducted in the presence of $MgSO_4$ with pH 2.0 and 4.0 in this work. In both the single arsenopyrite system and the mixed solution of arsenopyrite and $MgSO_4$, dissolved Fe(III) was detected under UV radiation (Fig. 5 and S6). The concentrations of As(T) and Fe(II) were respectively determined to be 52.5 and 65.2 μmol L^{-1}, 62.0 and 67.3 μmol L^{-1}, 69.3 and 69.2 μmol L^{-1}, at pH 2.0, 3.0 and 4.0 after 6 h of reaction in the single arsenopyrite system (Fig. 1 and S6). As for the mixed solution of arsenopyrite and $MgSO_4$, the concentrations of As(T) and Fe(II) were respectively 56.6 and 69.8 μmol L^{-1}, 90.5 and 94.0 μmol L^{-1}, 116.5 and 102.8 μmol L^{-1}, at pH 2.0, 3.0 and 4.0 after 6 h of reaction (Figs. 1 and 5). The above results indicated that the photochemical oxidation rate of arsenopyrite increases with increasing pH in the range of 2.0–4.0. It was also noted that there was no significant difference in the photochemical oxidation of arsenopyrite in the presence of SO_4^{2-} at pH 2.0. However, the presence of SO_4^{2-} significantly increased the photooxidation rate of arsenopyrite at pH 3.0 and 4.0. To further clarify the influence of UV radiation, the oxidation of arsenopyrite was also studied at pH 2.0 and 4.0 under dark conditions (Fig. S7), and the oxidation rate of arsenopyrite also increased with increasing pH. To better understand the arsenopyrite oxidation, the concentrations of As and Fe species released from arsenopyrite in all reaction systems after 6 h are summarized in Table S1.

In the mixed system of arsenopyrite and 5.0 mmol L^{-1} $MgSO_4$, the effect of oxygen was further investigated at pH 3.0 in the nitrogen atmosphere (Fig. 6). Under UV radiation, the maximum concentration of As(T) and Fe(II) (11.3 and 14.1 μmol L^{-1}, respectively) in nitrogen atmosphere was significantly lower than that in air atmosphere (90.5 and 94.0 μmol L^{-1}, respectively); and dissolved As(III) was the dominant dissolved As species, which was different from the results in air atmosphere (Figs. 1 and 6a, b). Under dark conditions, the oxidative dissolution rate of arsenopyrite was also significantly inhibited (Fig. 6c, d). The above results indicated that dissolved oxygen can significantly influence the oxidation of arsenopyrite and the further oxidation of As.

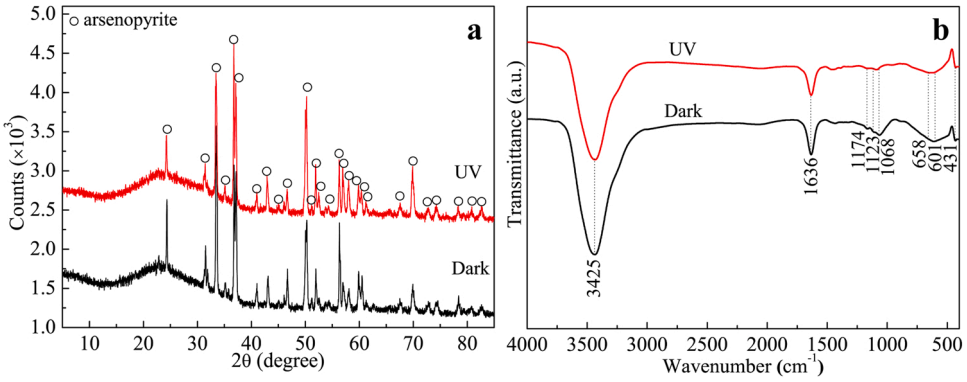

Fig. 2. XRD patterns (a) and FTIR spectra (b) of the solid products formed in the mixed system of arsenopyrite (0.5 g L^{-1}) and $MgSO_4$ (5.0 mmol L^{-1}) at pH 3.0 after 6 h in air atmosphere under UV radiation and dark conditions.

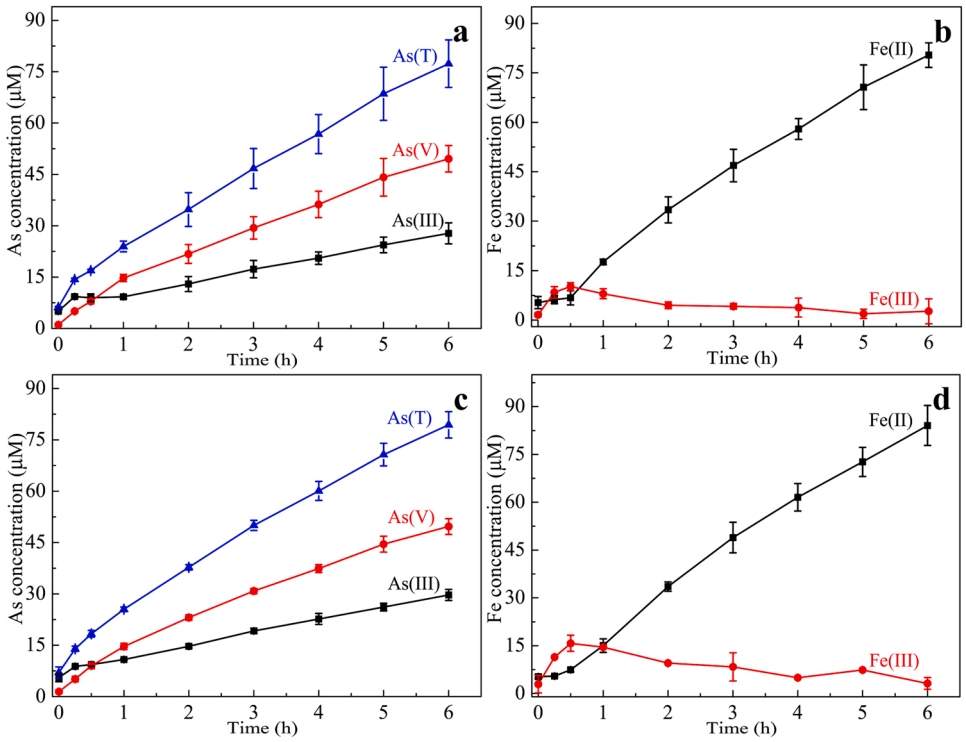

Fig. 3. Concentrations of dissolved As and Fe species in the mixed system of arsenopyrite (0.5 g L^{-1}) and $MgSO_4$ (1.0 mmol L^{-1}) (a, b) or $MgSO_4$ (10.0 mmol L^{-1}) (c, d) under UV radiation at pH 3.0 in air atmosphere.

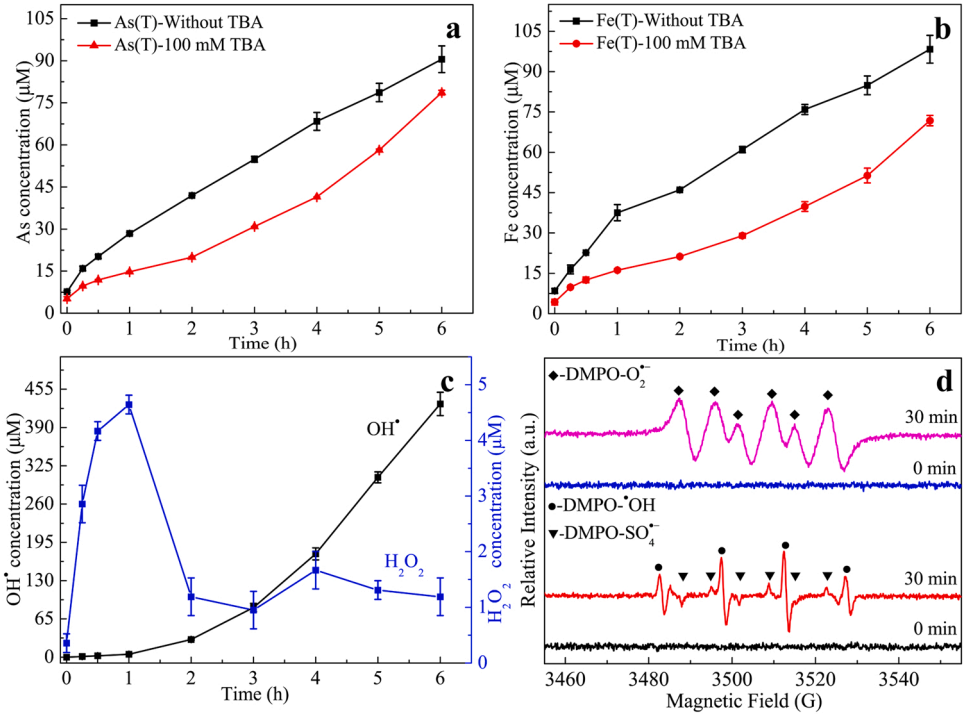

Fig. 4. Concentrations of dissolved As(T) (a) and Fe(T) (b) with or without the addition of 0.1 mol L^{-1} TBA, and cumulative concentration of •OH and instant concentration of H_2O_2 (c), and EPR spectra of •OH, $SO_4^{\bullet-}$ and $O_2^{\bullet-}$ (d) in the mixed system of arsenopyrite (0.5 g L^{-1}) and $MgSO_4$ (5.0 mmol L^{-1}) under UV radiation at pH 3.0 in air atmosphere.

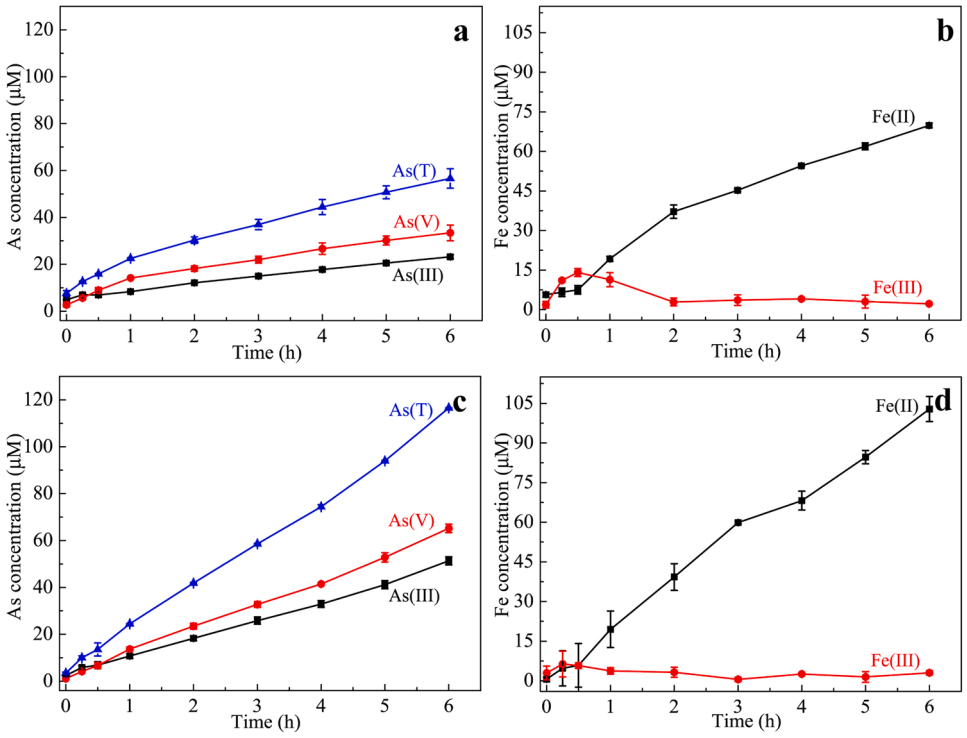

Fig. 5. Concentrations of dissolved As and Fe species in the mixed systems of arsenopyrite (0.5 g L^{-1}) and $MgSO_4$ (5.0 mmol L^{-1}) under UV radiation at pH 2.0 (a, b) and 4.0 (c, d) in air atmosphere.

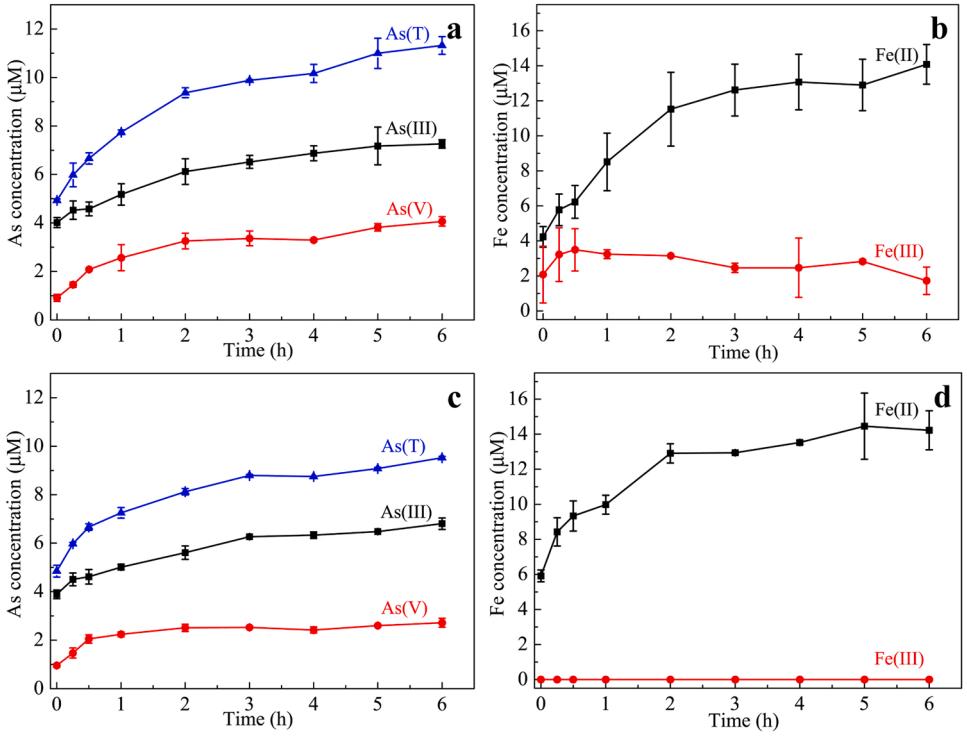

Fig. 6. Concentrations of dissolved As and Fe species in the mixed systems of arsenopyrite (0.5 g L^{-1}) and $MgSO_4$ (5.0 mmol L^{-1}) at pH 3.0 in nitrogen atmosphere under UV radiation (a, b) and dark conditions (c, d).

4. Discussion

4.1. Mechanism for the sulfate-induced photochemical oxidation of arsenopyrite

In earth's surface environments, solar radiation can strengthen the weathering of iron sulfide minerals. Our previous results have indicated that UV radiation accelerates the arsenopyrite oxidation by the generation of ROS under acidic conditions. In this process, $O_2^{\bullet-}$ is produced due to the excitation of As(III) by far-UV in the presence of O_2, and $^{\bullet}OH$ intermediates are formed through the photo-Fenton reaction (Fe(II)/$FeOH^{2+}$) under near-UV radiation (Hong et al., 2018). In this work, near-UV radiation was provided by a LED-UV lamp (Fig. S2), and the photo-Fenton reaction would occur in the reaction system. Therefore, in the single arsenopyrite system, UV radiation could significantly accelerate the oxidation rate of arsenopyrite, which may be attributed to the production of ROS from the photo-Fenton reaction.

Under UV radiation, the presence of $MgSO_4$ significantly increased the oxidation rate of arsenopyrite at pH 3.0 (Figs. 1 and 3). To elucidate this process, 10.0 mmol L^{-1} Na_2SO_4 was added to the arsenopyrite suspension under pH 3.0 in air atmosphere. As a result, the concentration of released As from arsenopyrite was not obviously different from that after the addition of 10.0 mmol L^{-1} $MgSO_4$ (Fig. 3 and S8). Then, $MgCl_2$ solutions (0 and 2.5 mmol L^{-1}) were added to the arsenopyrite suspension, and the pH was adjusted to 4.0 with 0.05–0.5 mol L^{-1} HCl (Fig. 7 and S9). It was observed that the addition of $MgCl_2$ resulted in significantly lower As(T) and Fe(II) concentrations after 6 h relative to the addition of $MgSO_4$ (Figs. 5 and 7). Therefore, only SO_4^{2-} could promote the photochemical oxidation of arsenopyrite in this work.

As(III,V) can be adsorbed through electrostatic attraction on the surface of sulfide minerals, iron (hydr)oxides and aluminum oxides (Bostick and Fendorf, 2003; Bostick et al., 2003; Jain and Loeppert, 2000). Many oxygen-containing anions including PO_4^{3-}, SO_4^{2-} and HCO_3^- have the same or higher charge density than arsenate and arsenite, and thus can decrease the adsorption capacity and improve the mobility of As(III,V) through competitive adsorption (ion exchange) (Cheng et al., 2009; Wilkie and Hering, 1996; Xu et al., 1988). In this study, at pH 3.0, the presence of SO_4^{2-} showed no obvious effect on the release rate of dissolved As(T) and Fe(II) from these reaction systems under dark conditions (Figs. S3 and S5), but significantly increased the release of dissolved As(T) and Fe(II) under UV radiation (Figs. 1 and 3). Therefore, the possible ion exchange between SO_4^{2-} and As-containing anions may not contribute much to the photochemical oxidation of arsenopyrite.

The photochemical oxidation pathway mediated by SO_4^{2-} can accelerate the oxidative dissolution of arsenopyrite. Under near-UV radiation, the arsenopyrite photooxidation is mainly affected by the photo-Fenton reaction in the absence of high concentration coexisting anions (Hong et al., 2018). At pH < 5.0, SO_4^{2-} will compete with OH^- for Fe(III) coordination, and $FeSO_4^+$ was the preponderant species when a high concentration of SO_4^{2-} was added to the solution (Machulek et al., 2009) (Fig. S10). Although $FeSO_4^+$ has certain photoactivity, the active free radical $SO_4^{\bullet-}$ can be formed due to the photo-decomposition with a quantum yield as low as 0.0016 (λ = 350 nm), which is significantly lower than that of $FeOH^{2+}$ (0.21, λ = 347 nm) (Machulek et al., 2009). As reported, $FeSO_4^+$ has a lower photoactivity than $FeOH^{2+}$ (Benkelberg and Warneck, 1995; Machulek et al., 2009). In this work, although $SO_4^{\bullet-}$ was detected in the mixed system under UV radiation, the relative intensity of the peaks of $SO_4^{\bullet-}$ was significantly lower than that of $^{\bullet}OH$ (Fig. 4d). Therefore, $FeSO_4^+$ may have little contribution to the promotion effect of SO_4^{2-} on the photochemical oxidation of arsenopyrite in the mixed system.

In the AMD environment, Fe(III) and high-concentration SO_4^{2-} facilitate the formation of schwertmannite, which can stably exist in the pH range of 2.5–4.5 (Bigham et al., 1990, 1996). Moreover, the presence of ROS can promote the formation of schwertmannite in $FeSO_4$ solution (Paikaray et al., 2011; Regenspurg et al., 2004). In this work, ROS including $^{\bullet}OH$ and H_2O_2 were detected at pH 3.0 under UV radiation, and dissolved Fe(II) was the dominant Fe species in the mixed system (Figs. 1b and 4). Only arsenopyrite but no schwertmannite was detected

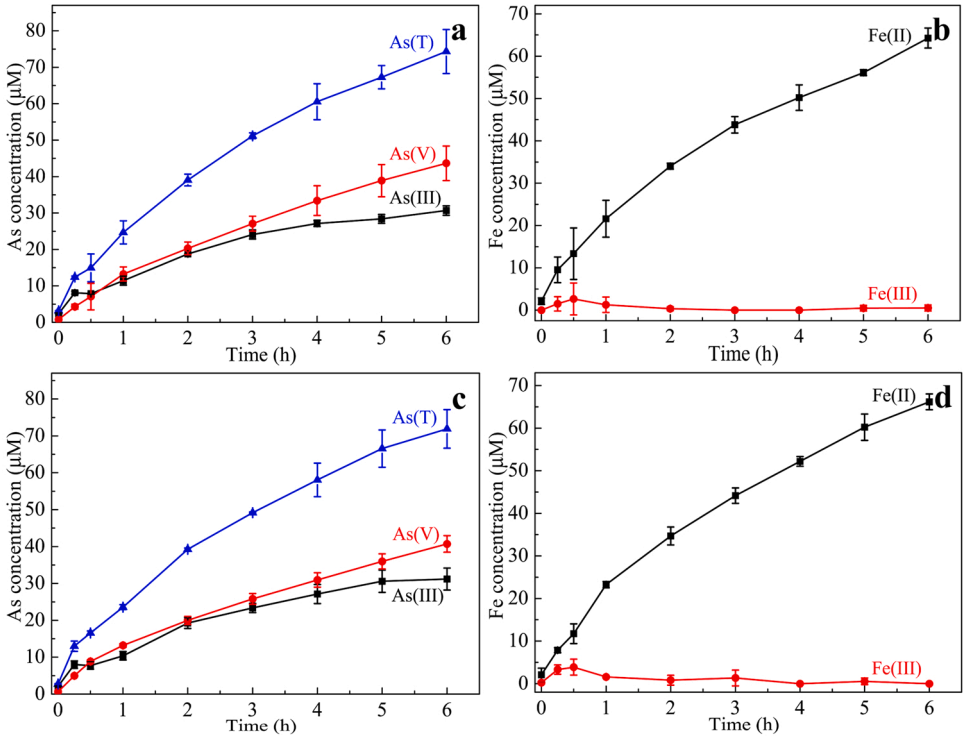

Fig. 7. Concentrations of dissolved As and Fe species in the mixed system of arsenopyrite (0.5 g L^{-1}) and $MgCl_2$ (2.5 mmol L^{-1}) (a, b), and in the single arsenopyrite (0.5 g L^{-1}) system (c, d) under UV radiation at pH 4.0 in air atmosphere. The initial pH of these reaction systems was adjusted with HCl.

in the solid products as indicated by XRD and FTIR, possibly due to the small amount and weak crystallinity of schwertmannite in the system (Fig. 2). In order to check the possible formation of schwertmannite, Fe K-edge EXAFS spectrum was further used to analyze the chemical composition of the solid products in the mixed system containing 10.0 mmol L^{-1} $MgSO_4$ after 12 h at pH 3.0 in air atmosphere under UV radiation. Schwertmannite was detected on the arsenopyrite surface with a relative content of 2.1% (± 0.004) (Fig. 8) (Supporting Information SII), suggesting that schwertmannite was formed possibly through the oxidization of Fe(II) and SO_4^{2-} by ROS under UV radiation.

Dissolved As(III) and Sb(III) can complex with ferrihydrite (ferrihydrite–As(III)/Sb(III)) in nearly neutral pH environments. Ferrihydrite–As(III)/Sb(III) can absorb UV radiation, and induce electron transfer between Fe(III) in ferrihydrite and As(III)/Sb(III) by the LMCT process, facilitating the oxidation of As(III)/Sb(III). In addition, oxygen is reduced to form superoxide radical ($O_2^{\bullet-}$/$HO_2^{\bullet}$) (Kong et al., 2016; Xu et al., 2014). As reported, As(III) can complex with schwertmannite to form schwertmannite–As(III) (Zhang et al., 2019). Upon the occurrence of a LMCT process, a charge-transfer spectrum of schwertmannite–As(III) complex should be observed by UV−vis full band scanning (Mostafa et al., 2013). In this work, the UV−vis absorption spectra of As(III), schwertmannite and schwertmannite–As(III) complex were studied by UV−vis full band scanning at pH 3.0 (Fig. 9 and S11) (Supporting Information SIII). No obvious absorption was observed for 500 μmol L^{-1} As(III) at wavelengths above 250 nm, while absorption spectra of schwertmannite (0.05 g L^{-1}) were observed in both the UV and visible regions. The UV−vis adsorption spectra showed a gradually rising trend of absorption intensity in schwertmannite suspension with increasing As(III) concentration over a wide range of wavelengths from 250 to 600 nm. The absorption spectra of the schwertmannite suspension in the presence of As(III) showed a deflection point at 290 nm, which is similar to previous reports (Kong et al., 2016; Xu et al., 2014). At λ = 290 nm, the absorption spectral data of schwertmannite suspension in the presence of As(III) were fitted by using the Benesi−Hildebrand equation (Fig. 9) (Supporting Information SIII). The good linear relationship confirmed the formation of schwertmannite–As(III) complex and the occurrence of LMCT process between Fe(III) and As(III) inside the complex. Moreover, $O_2^{\bullet-}$ was detected in the mixed system under UV radiation (Fig. 4d). Therefore, the promotion of photooxidation of arsenopyrite and low-valence As by SO_4^{2-} is very likely due to the formation of complex between the nascent schwertmannite and dissolved As(III). The complexed As(III) was photochemically oxidized to As(V) through the LMCT process, which is accompanied by the generation of ROS in the presence of O_2.

Galvanic interaction is a well-known phenomenon observed in mine drainage formation, sulfide mineral processing and flotation (Chopard et al., 2017; Jeon et al., 2020; Seng et al., 2019). Previous studies have shown that hematite can enhance the anode oxidation of pyrite through electron "bridging" and catalytic effects (Tabelin et al., 2017c). The direct contact of sulfide minerals with different rest potentials, such as pyrite and chalcopyrite, pyrite and sphalerite, will initiate the galvanic effect to accelerate the oxidation of sulfide minerals (Chopard et al., 2017). Therefore, the galvanic interaction between arsenopyrite and nascent schwertmannite may also occur with a subsequent increase in the oxidative dissolution of arsenopyrite in this work. The exact process and mechanism still need to be further studied in the future.

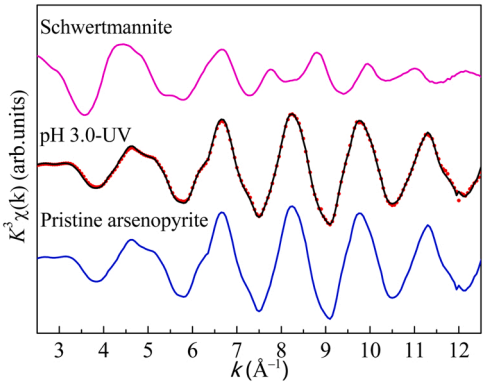

Fig. 8. Fe K-edge EXAFS spectra (red dotted lines) and the corresponding linear combination fitting (gray solid lines) of the solid products formed in the mixed system of arsenopyrite (0.5 g L^{-1}) and $MgSO_4$ (10.0 mmol L^{-1}) after 12 h at pH 3.0 in air atmosphere under UV radiation.

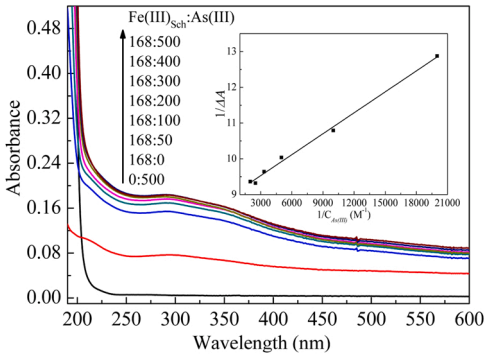

Fig. 9. UV−vis absorption spectra of schwertmannite−As(III) complex at pH 3.0 using quartz cell with the thickness of 1.0 cm. The inset shows the Benesi–Hildebrand plot fitting for the schwertmannite−As(III) complex at 290 nm. [Fe(III)] = 168 μM. Equation: $1/\Delta A = (1.95 \pm 0.07) \times 10^{-4} \times 1/C_{As(III)} + (8.95 \pm 0.06)$; $R^2 = 0.9944$.

Schwertmannite has excellent adsorption capacity for As, and has been widely studied for As removal from polluted natural environments (Burton et al., 2009); and UV radiation can facilitate the adsorption and fixation of As on schwertmannite surface (Ren et al., 2018; Zhang et al., 2019). AsO_4^{3-} can also substitute SO_4^{2-} in the crystal structure to form As-bearing schwertmannite during the aging of minerals (Regenspurg and Peiffer, 2005; Zhang et al., 2016b). In this study, the photooxidation rate of arsenopyrite first rose and then fell with increasing $MgSO_4$ concentration from 0 to 10.0 mmol L^{-1}, which was likely due to the adsorption of As on schwertmannite surface and incorporation of dissolved As into the crystal structure of schwertmannite.

4.2. Effects of pH and dissolved oxygen

Dissolved Fe(III) can directly participate in the weathering of arsenopyrite, especially in acidic solutions. Hence, the released Fe ions will further affect the oxidation of arsenopyrite (Yu et al., 2007; Yunmei et al., 2004). When the pH is below 5.0, the Fe^{2+} released from arsenopyrite will be oxidized to Fe^{3+} with increasing pH, which will further accelerate arsenopyrite oxidation (Yu et al., 2007). Therefore, in the pH range of 2.0–4.0, the gradual increase in the oxidation rate of arsenopyrite under dark conditions may be partly due to the accelerated formation of dissolved Fe^{3+}.

The pH has a direct impact on the complex species of Fe(III) and inorganic anions (Fig. S10) (Machulek et al., 2009). Low pH facilitates the formation of $FeSO_4^+$ and inhibits the photo-Fenton reaction of Fe(II)/$FeOH^{2+}$ (Fig. S10). In this work, the actual concentration of SO_4^{2-} was about 5.0, 0.5 and 0.05 mmol L^{-1} at pH 2.0, 3.0 and 4.0 in the single arsenopyrite system, respectively. The arsenopyrite photooxidation rate increased with increasing pH, which was likely due to the gradual decrease in SO_4^{2-} concentration and increase in the complexation capability of Fe^{3+} with OH^-.

The pH also affects the formation process and chemical stability of schwertmannite. At pH < 2.5, the formation of schwertmannite will be inhibited, and schwertmannite is easily transformed into other more stable iron (hydr)oxides including goethite at pH > 4.5 (Jönsson et al.,

2005; Knorr and Blodau, 2007). The formation of schwertmannite is accompanied by the release of H^+. Within a suitable pH range, a high pH can facilitate the formation of schwertmannite (Regenspurg et al., 2004; Su et al., 2019). The presence of SO_4^{2-} at pH 2.0 under UV radiation did not obviously affect the oxidation rate of arsenopyrite likely due to the difficulty in the formation of schwertmannite (Fig. 5 and S6). However, the As(T) concentration after 6 h in the mixed system was 1.5 and 1.7 folds of that in the single system at pH 3.0 and 4.0, respectively (Figs. 1, 5 and S6). SO_4^{2-} significantly accelerated the oxidation of arsenopyrite, suggesting that schwertmannite tends to be formed at pH 3.0 and 4.0. Compared with pH 3.0, pH 4.0 facilitated the formation of $FeOH^{2+}$ (Fig. S10). In this work, the release rate of As from arsenopyrite increased progressively with increasing pH in the mixed system of arsenopyrite and $MgSO_4$ under UV radiation, possibly because the effect of pH on schwertmannite formation rate and photo-Fenton reaction follows the order of pH 4.0 > pH 3.0 > > pH 2.0.

Oxygen usually works as the ultimate electron acceptor for the redox reaction in nature, and plays an important role in the geochemical cycle of many elements. The heterogeneous oxidation reaction of As(III) with ROS as the intermediate products is a key process for the rapid oxidation of As(III) in the presence of O_2 (Cheng et al., 2009; Hong et al., 2021). Our previous work has demonstrated that O_2 can accelerate the oxidative dissolution of arsenopyrite and the further oxidation of dissolved As (III) through promoting the ROS formation during the (photo)oxidation of arsenopyrite (Hong et al., 2018, 2020, 2021). In this work, oxygen facilitates the formation of $O_2^{\bullet-}/HO_2^{\bullet}$ from the LMCT process, promoting the photooxidation of arsenopyrite and As(III). $O_2^{\bullet-}/HO_2^{\bullet}$ could be converted to form H_2O_2. Therefore, a higher content of $O_2^{\bullet-}/HO_2^{\bullet}$ may indicate an increase in the content of H_2O_2 in the reaction system, which further promotes the photo-Fenton reaction.

In our previous work, due to the presence of trace oxides on the arsenopyrite surface, the released As from arsenopyrite oxidation mainly exists as As(V) due to photo-Fenton reaction in the absence of high-concentration SO_4^{2-} at pH 3.0 in nitrogen atmosphere (Hong et al., 2018). In this work, in the presence of a higher concentration of SO_4^{2-}, $FeSO_4^+$ could inhibit the formation of $FeOH^{2+}$, followed by the inhibition of the photo-Fenton reaction. The absence of O_2 as an electron acceptor would also inhibit the LMCT process (Kong et al., 2016; Xu et al., 2014). Therefore, the dissolved As from arsenopyrite mainly exists as As(III) at pH 3.0 under UV radiation in nitrogen atmosphere (Fig. 6a).

4.3. Environmental significance

Excessive discharge of AMD has caused serious environmental and ecological problems, and it is almost impossible to prevent its generation (Rodríguez-Galán et al., 2019). Arsenopyrite is one of the most common iron sulfide minerals, and its oxidation is a major source of AMD, causing serious As pollution to the environment. Therefore, it is of great significance to comprehensively understand the oxidation and dissolution of arsenopyrite in the AMD environment for a better control of As pollution.

Large amounts of inorganic anions including Cl^-, NO_3^-, PO_4^{3-} and SO_4^{2-} are present in AMD or natural waters (Cheng et al., 2009). The dissolution rate of sulfur in sulfide minerals (arsenopyrite, galena and pyrite) decreases with increasing Cl^- activity under anoxic and acidic conditions (Parthasarathy et al., 2015). Compared with $Fe_2(SO_4)_3$, $FeCl_3$ shows a higher arsenopyrite oxidation activity (Yunmei et al., 2004). As a matter of fact, PO_4^{3-} and SO_4^{2-} have competitive adsorption with As (III,V) on the mineral surface, which will obviously affect the migration of As in the environment (Cheng et al., 2009; Wilkie and Hering, 1996). These findings indicate that inorganic anions significantly affect the weathering of sulfide minerals and the fate of As (Cheng et al., 2009; Yunmei et al., 2004).

Sulfide minerals are exposed to solar irradiation in the earth's surface environment. Iron (hydr)oxides including schwertmannite and goethite usually exhibit excellent adsorption capacity for As. Hence, current research has been mostly focused on the influence of iron (hydr) oxides on the migration of As in the AMD environment (Burton et al., 2009; Cheng et al., 2009). However, little attention has been paid to the effect of photoreactivity of schwertmannite on the oxidation of sulfide minerals. Besides, field surveys have demonstrated that As(V) works as the preponderant species and associated with schwertmannite, while both As(III) and As(V) are present in the streams of the mining area, which may be ascribed to the direct adsorption of As(V) or the oxidation of the adsorbed As(III) to As(V) on schwertmannite (Asta et al., 2010; Paikaray, 2015). In this work, it was noted that the presence of high-concentration SO_4^{2-} could accelerate the photooxidation of arsenopyrite and As(III). At pH 3.0 and 4.0, the concentration of released As (T) was increased respectively by 46.0% and 68.1% in the mixed system of arsenopyrite (0.5 g L^{-1}) and $MgSO_4$ (5.0 mmol L^{-1}) compared with that in the single arsenopyrite system under UV radiation. In this process, the newly formed schwertmannite plays an important role in the photooxidation of arsenopyrite and As(III). Previous studies were usually concerned about the adsorption and fixation of dissolved As. This work provides some new insights into the oxidation of sulfide minerals and the release of As, and a new pathway to understand the phenomenon that adsorbed As(V) is the predominant As species in schwertmannite in the field survey. As a common anion, SO_4^{2-} accelerates the oxidation of arsenopyrite under solar radiation. Therefore, besides adjusting pH, decreasing the concentration of SO_4^{2-} and avoiding solar radiation should be recommended for decreasing the environmental risk of AMD.

5. Conclusions

SO_4^{2-} accelerates the photooxidation of arsenopyrite under UV radiation. Under UV radiation, Fe(II) released from arsenopyrite and high-concentration SO_4^{2-} are oxidized by ROS to form schwertmannite. Dissolved As(III) is adsorbed on nascent schwertmannite to form schwertmannite–As(III) complex, and the photooxidation of arsenopyrite and As(III) occurs through the LMCT process along with the generation of ROS in the presence of O_2. The photooxidation rate of arsenopyrite first rises and then falls with increasing $MgSO_4$ concentration from 0 to 10.0 mmol L^{-1} in this process. In the pH range of 2.0–4.0, the inhibitory effect of $FeSO_4^+$ on the photo-Fenton reaction gradually decreases and the production rate of schwertmannite gradually increases, resulting in a progressive increase in the photooxidation rate of arsenopyrite. Dissolved oxygen is the main electron acceptor in the redox reaction of arsenopyrite, and significantly affects the oxidation of arsenopyrite and release of As.

CRediT authorship contribution statement

Jun Hong: Investigation, Writing – original draft, Writing – review & editing. **Lihu Liu**: Validation, Writing – review & editing. **Ziwei Zhang**: Validation. **Xiange Xia**: Conceptualization, Writing – review & editing, Supervision, Project administration. **Li Yang**: Funding acquisition. **Zengping Ning**: Resources. **Chengshuai Liu**: Resources, Funding acquisition. **Guohong Qiu**: Conceptualization, Writing – review & editing, Supervision, Funding acquisition, Project administration.

Declaration of Competing Interest

The authors declare that they have no known competing financial interests or personal relationships that could have appeared to influence the work reported in this paper.

Acknowledgments

This work was financially supported by the National Natural Science Foundation of China (Grant Nos. 41877025, 42077133 and 42007127) and the National Key Research and Development Program of China (No.

2020YFC1808503), Leading Talent of "Ten Thousand Plan"-National High-Level Talents Special Support Plan, West Light Foundation and the Frontier Science Research Programme of the Chinese Academy of Sciences (QYZDB-SSW-DQC046), the National Key Research and Development Program of China (No. 2017YFD0801003), and the Non-profit Collaborative Innovation Alliance Project (2018LM). This work was carried out with the support of 1W1B beamline at Beijing Synchrotron Radiation Facility. The authors owe thank Lihong Qin and Jianbo Cao at Public Laboratory of Electron Microscope of Huazhong Agricultural University for SEM analyses.

Novelty Statement

Arsenopyrite is one of the most common arsenic (As)-containing iron sulfide minerals, and its weathering is an important factor leading to the generation of acid mine drainage (AMD) and As pollution. Our previous work has shown that solar radiation can promote arsenopyrite oxidation and As release. However, the effect of SO_4^{2-} on the photooxidation of arsenopyrite in the AMD environment remains elusive. This work systematically studied the mechanism for $SO_{4^{2-}}$ to promote arsenopyrite photooxidation in simulated AMD environments. The findings can provide some new theoretical guidance for the environmental management of AMD as well as the treatment of As pollution.

Appendix A. Supporting information

Supplementary data associated with this article can be found in the online version at doi:10.1016/j.jhazmat.2022.128716.

References

Aikawa, K., Ito, M., Segawa, T., Jeon, S., Park, I., Tabelin, C.B., Hiroyoshi, N., 2020. Depression of lead-activated sphalerite by pyrite via galvanic interactions: Implications to the selective flotation of complex sulfide ores. Miner. Eng. 152, 106367.

Asta, M.P., Ayora, C., Román-Ross, G., Cama, J., Acero, P., Gault, A.G., Charnock, J.M., Bardelli, F., 2010. Natural attenuation of arsenic in the Tinto Santa Rosa acid stream (Iberian Pyritic Belt, SW Spain): the role of iron precipitates. Chem. Geol. 271, 1–12.

Bagchi, S., 2007. Arsenic threat reaching global dimensions. Can. Med. Assoc. J. 177, 1344–1345.

Benkelberg, H.-J., Warneck, P., 1995. Photodecomposition of iron(III) hydroxo and sulfato complexes in aqueous solution: wavelength dependence of OH and SO_4^- quantum yields. J. Phys. Chem. 99, 5214–5221.

Bigham, J.M., Schwertmann, U., Carlson, L., Murad, E., 1990. A poorly crystallized oxyhydroxysulfate of iron formed by bacterial oxidation of Fe(II) in acid-mine waters. Geochim. Cosmochim. Acta 54, 2743–2758.

Bigham, J.M., Schwertmann, U., Traina, S.J., Winland, R.L., Wolf, M., 1996. Schwertmannite and the chemical modeling of iron in acid sulfate waters. Geochim. Cosmochim. Acta 60, 2111–2121.

Borda, M.J., Strongin, D.R., Schoonen, M.A., 2004. A vibrational spectroscopic study of the oxidation of pyrite by molecular oxygen. Geochim. Cosmochim. Acta 68, 1807–1813.

Bostick, B.C., Fendorf, S., 2003. Arsenite sorption on troilite (FeS) and pyrite (FeS_2). Geochim. Cosmochim. Acta 67, 909–921.

Bostick, B.C., Fendorf, S., Manning, B.A., 2003. Arsenite adsorption on galena (PbS) and sphalerite (ZnS). Geochim. Cosmochim. Acta 67, 895–907.

Burton, E.D., Bush, R.T., Johnston, S.G., Watling, K.M., Hocking, R.K., Sullivan, L.A., Parker, G.K., 2009. Sorption of arsenic(V) and arsenic(III) to schwertmannite. Environ. Sci. Technol. 43, 9202–9207.

Cheng, H., Hu, Y., Luo, J., Xu, B., Zhao, J., 2009. Geochemical processes controlling fate and transport of arsenic in acid mine drainage (AMD) and natural systems. J. Hazard. Mater. 165, 13–26.

Chopard, A., Plante, B., Benzaazoua, M., Bouzahzah, H., Marion, P., 2017. Geochemical investigation of the galvanic effects during oxidation of pyrite and base-metals sulfides. Chemosphere 166, 281–291.

Chu, L., Anastasio, C., 2003. Quantum yields of hydroxyl radical and nitrogen dioxide from the photolysis of nitrate on ice. J. Phys. Chem. A 107, 9594–9602.

Emett, M.T., Khoe, G.H., 2001. Photochemical oxidation of arsenic by oxygen and iron in acidic solutions. Water Res 35, 649–656.

Gray, N.F., 1998. Acid mine drainage composition and the implications for its impact on lotic systems. Water Res 32, 2122–2134.

Guo, J., Dong, C., Zhang, J., Lan, Y., 2015. Biogenic synthetic schwertmannite photocatalytic degradation of acid orange 7 (AO7) assisted by citric acid. Sep. Purif. Technol. 143, 27–31.

Heviánková, S., Bestová, I., Kyncl, M., 2014. The application of wood ash as a reagent in acid mine drainage treatment. Miner. Eng. 56, 109–111.

Hong, J., Liu, L., Luo, Y., Tan, W., Qiu, G., Liu, F., 2018. Photochemical oxidation and dissolution of arsenopyrite in acidic solutions. Geochim. Cosmochim. Acta 239, 173–185.

Hong, J., Liu, L., Ning, Z., Liu, C., Qiu, G., 2021. Synergistic oxidation of dissolved As(III) and arsenopyrite in the presence of oxygen: Formation and function of reactive oxygen species. Water Res 202, 117416.

Hong, J., Liu, L., Tan, W., Qiu, G., 2020. Arsenic release from arsenopyrite oxidative dissolution in the presence of citrate under UV irradiation. Sci. Total Environ. 726, 138429.

Igarashi, T., Herrera, P.S., Uchiyama, H., Miyamae, H., Iyatomi, N., Hashimoto, K., Tabelin, C.B., 2020. The two-step neutralization ferrite-formation process for sustainable acid mine drainage treatment: Removal of copper, zinc and arsenic, and the influence of coexisting ions on ferritization. Sci. Total Environ. 715, 136877.

Jain, A., Loeppert, R.H., 2000. Effect of competing anions on the adsorption of arsenate and arsenite by ferrihydrite. J. Environ. Qual. 29, 1422–1430.

Jeon, S., Tabelin, C.B., Takahashi, H., Park, I., Ito, M., Hiroyoshi, N., 2020. Enhanced cementation of gold via galvanic interactions using activated carbon and zero-valent aluminum: A novel approach to recover gold ions from ammonium thiosulfate medium. Hydrometallurgy 191, 105165.

Jönsson, J., Persson, P., Sjöberg, S., Lövgren, L., 2005. Schwertmannite precipitated from acid mine drainage: phase transformation, sulphate release and surface properties. Appl. Geochem. 20, 179–191.

Kaplun, K., Li, J., Kawashima, N., Gerson, A.R., 2011. Cu and Fe chalcopyrite leach activation energies and the effect of added Fe^{3+}. Geochim. Cosmochim. Acta 75, 5865–5878.

Kerr, J.B., Fioletov, V.E., 2008. Surface ultraviolet radiation. Atmos. Ocean 46, 159–184.

Knorr, K.-H., Blodau, C., 2007. Controls on schwertmannite transformation rates and products. Appl. Geochem. 22, 2006–2015.

Kong, L., He, M., Hu, X., 2016. Rapid photooxidation of Sb(III) in the presence of different Fe(III) species. Geochim. Cosmochim. Acta 180, 214–226.

Lee, H., Choi, W., 2002. Photocatalytic oxidation of arsenite in TiO_2 suspension: kinetics and mechanisms. Environ. Sci. Technol. 36, 3872–3878.

Liu, L., Jia, Z., Tan, W., Suib, S.L., Ge, L., Qiu, G., Hu, R., 2018. Abiotic photomineralization and transformation of iron oxide nanominerals in aqueous systems. Environ. Sci.: Nano 5, 1169–1178.

Liu, Q., Li, H., Zhou, L., 2008. Galvanic interactions between metal sulfide minerals in a flowing system: Implications for mines environmental restoration. Appl. Geochem. 23, 2316–2323.

Machulek Jr, A., Moraes, J.E.F., Okano, L.T., Silverio, C.A., Quina, F.H., 2009. Photolysis of ferric ions in the presence of sulfate or chloride ions: implications for the photo-Fenton process. Photochem. Photobiol. Sci. 8, 985–991.

Mack, J., Bolton, J.R., 1999. Photochemistry of nitrite and nitrate in aqueous solution: a review. J. Photochem. Photobiol., A 128, 1–13.

Mazumdar, A., Goldberg, T., Strauss, H., 2008. Abiotic oxidation of pyrite by Fe(III) in acidic media and its implications for sulfur isotope measurements of lattice-bound sulfate in sediments. Chem. Geol. 253, 30–37.

Mikhlin, Y.L., Romanchenko, A.S., Asanov, I.P., 2006. Oxidation of arsenopyrite and deposition of gold on the oxidized surfaces: A scanning probe microscopy, tunneling spectroscopy and XPS study. Geochim. Cosmochim. Acta 70, 4874–4888.

Mostafa, A., El-Ghossein, N., Cieslinski, G.B., Bazzi, H.S., 2013. UV–Vis, IR spectra and thermal studies of charge transfer complexes formed in the reaction of 4-benzylpiperidine with σ-and π-electron acceptors. J. Mol. Struct. 1054–1055, 199–208.

Murciego, A., Álvarez-Ayuso, E., Pellitero, E., Rodríguez, M.A., García-Sánchez, A., Tamayo, A., Rubio, J., Rubio, F., Rubin, J., 2011. Study of arsenopyrite weathering products in mine wastes from abandoned tungsten and tin exploitations. J. Hazard. Mater. 186, 590–601.

Nansai, K., Nakajima, K., Kagawa, S., Kondo, Y., Suh, S., Shigetomi, Y., Oshita, Y., 2014. Global flows of critical metals necessary for low-carbon technologies: the case of neodymium, cobalt, and platinum. Environ. Sci. Technol. 48, 1391–1400.

Neil, C.W., Jun, Y.-S., 2016. Fe^{3+} addition promotes arsenopyrite dissolution and iron (III) (hydr)oxide formation and phase transformation. Environ. Sci. Technol. Lett. 3, 30–35.

Nimick, D.A., Gammons, C.H., Cleasby, T.E., Madison, J.P., Skaar, D., Brick, C.M., 2003. Diel cycles in dissolved metal concentrations in streams: occurrence and possible causes. Water Resour. Res. 39, 1247.

Nimick, D.A., Gammons, C.H., Parker, S.R., 2011. Diel biogeochemical processes and their effect on the aqueous chemistry of streams: A review. Chem. Geol. 283, 3–17.

Paikaray, S., 2015. Arsenic geochemistry of acid mine drainage. Mine Water Environ. 34, 181–196.

Paikaray, S., Göttlicher, J., Peiffer, S., 2011. Removal of As(III) from acidic waters using schwertmannite: Surface speciation and effect of synthesis pathway. Chem. Geol. 283, 134–142.

Park, I., Higuchi, K., Tabelin, C.B., Jeon, S., Ito, M., Hiroyoshi, N., 2021. Suppression of arsenopyrite oxidation by microencapsulation using ferric-catecholate complexes and phosphate. Chemosphere 269, 129413.

Parthasarathy, H., Dzombak, D.A., Karamalidis, A.K., 2015. Alkali and alkaline earth metal chloride solutions influence sulfide mineral dissolution. Chem. Geol. 412, 26–33.

Qiu, G., Luo, Y., Chen, C., Lv, Q., Tan, W., Liu, F., Liu, C., 2016. Influence factors for the oxidation of pyrite by oxygen and birnessite in aqueous systems. J. Environ. Sci. 45, 164–176.

Regenspurg, S., Brand, A., Peiffer, S., 2004. Formation and stability of schwertmannite in acidic mining lakes. Geochim. Cosmochim. Acta 68, 1185–1197.

Regenspurg, S., Peiffer, S., 2005. Arsenate and chromate incorporation in schwertmannite. Appl. Geochem. 20, 1226–1239.

Ren, H.T., Ji, Z.Y., Wu, S.H., Han, X., Liu, Z.M., Jia, S.Y., 2018. Photoreductive dissolution of schwertmannite induced by oxalate and the mobilization of adsorbed As(V). Chemosphere 208, 294–302.
Rodríguez-Galán, M., Baena-Moreno, F.M., Vázquez, S., Arroyo-Torralvo, F., Vilches, L. F., Zhang, Z., 2019. Remediation of acid mine drainage. Environ. Chem. Lett. 17, 1529–1538.
Ryu, J., Monllor-Satoca, D., Kim, D., Yeo, J., Choi, W., 2013. Photooxidation of arsenite under 254 nm irradiation with a quantum yield higher than unity. Environ. Sci. Technol. 47, 9381–9387.
Sarmiento, A.M., Oliveira, V., Gǿmez-Ariza, J.L., Nieto, J.M., Sańchez-Rodas, D., 2007. Diel cycles of arsenic speciation due to photooxidation in acid mine drainage from the Iberian Pyrite Belt (Sw Spain). Chemosphere 66, 677–683.
Seng, S., Tabelin, C.B., Makino, Y., Chea, M., Phengsaart, T., Park, I., Hiroyoshi, N., Ito, M., 2019. Improvement of flotation and suppression of pyrite oxidation using phosphate-enhanced galvanic microencapsulation (GME) in a ball mill with steel ball media. Miner. Eng. 143, 105931.
Singh, R., Singh, S., Parihar, P., Singh, V.P., Prasad, S.M., 2015. Arsenic contamination, consequences and remediation techniques: a review. Ecotoxicol. Environ. Saf. 112, 247–270.
Su, X., Li, X., Ma, L., Fan, J., 2019. Formation and transformation of schwertmannite in the classic Fenton process. J. Environ. Sci. 82, 145–154.
Tabelin, C.B., Corpuz, R.D., Igarashi, T., Villacorte-Tabelin, M., Alorro, R.D., Yoo, K., Raval, S., Ito, M., Hiroyoshi, N., 2020b. Acid mine drainage formation and arsenic mobility under strongly acidic conditions: Importance of soluble phases, iron oxyhydroxides/oxides and nature of oxidation layer on pyrite. J. Hazard. Mater. 399, 122844.
Tabelin, C.B., Igarashi, T., Villacorte-Tabelin, M., Park, I., Opiso, E.M., Ito, M., Hiroyoshi, N., 2018. Arsenic, selenium, boron, lead, cadmium, copper, and zinc in naturally contaminated rocks: a review of their sources, modes of enrichment, mechanisms of release, and mitigation strategies. Sci. Total Environ. 645, 1522–1553.
Tabelin, C.B., Sasaki, R., Igarashi, T., Park, I., Tamoto, S., Arima, T., Ito, M., Hiroyoshi, N., 2017a. Simultaneous leaching of arsenite, arsenate, selenite and selenate, and their migration in tunnel-excavated sedimentary rocks: I. Column experiments under intermittent and unsaturated flow. Chemosphere 186, 558–569.
Tabelin, C.B., Silwamba, M., Paglinawan, F.C., Mondejar, A.J.S., Duc, H.G., Resabal, V.J., Opiso, E.M., Igarashi, T., Tomiyama, S., Ito, M., Hiroyoshi, N., Villacorte-Tabelin, M., 2020a. Solid-phase partitioning and release-retention mechanisms of copper, lead, zinc and arsenic in soils impacted by artisanal and small-scale gold mining (ASGM) activities. Chemosphere 260, 127574.
Tabelin, C.B., Veerawattananun, S., Ito, M., Hiroyoshi, N., Igarashi, T., 2017b. Pyrite oxidation in the presence of hematite and alumina: I. Batch leaching experiments and kinetic modeling calculations. Sci. Total Environ. 580, 687–689.
Tabelin, C.B., Veerawattananun, S., Ito, M., Hiroyoshi, N., Igarashi, T., 2017c. Pyrite oxidation in the presence of hematite and alumina: II. Effects on the cathodic and anodic half-cell reactions. Sci. Total Environ. 581, 126–135.
Thao, N.T.P., Tsuji, S., Jeon, S., Park, I., Tabelin, C.B., Ito, M., Hiroyoshi, N., 2020. Redox potential-dependent chalcopyrite leaching in acidic ferric chloride solutions: Leaching experiments. Hydrometallurgy 194, 105299.
Tomiyama, S., Igarashi, T., Tabelin, C.B., Tangviroon, P., Ii, H., 2020. Modeling of the groundwater flow system in excavated areas of an abandoned mine. J. Contam. Hydrol. 230, 103617.
Wang, S., Zheng, K., Li, H., Feng, X., Wang, L., Liu, Q., 2021. Arsenopyrite weathering in acidic water: Humic acid affection and arsenic transformation. Water Res 194, 116917.
Wei, Z.S., Villamena, F.A., Weavers, L.K., 2017. Kinetics and mechanism of ultrasonic activation of persulfate: an in situ EPR spin trapping study. Environ. Sci. Technol. 51, 3410–3417.
Wilkie, J.A., Hering, J.G., 1996. Adsorption of arsenic onto hydrous ferric oxide: effects of adsorbate/adsorbent ratios and co-occurring solutes. Colloids Surf. A 107, 97–110.
Wu, X., Burnell, S., Neil, C.W., Kim, D., Zhang, L., Jung, H., Jun, Y.-S., 2020. Effects of phosphate, silicate, and bicarbonate on arsenopyrite dissolution and secondary mineral precipitation. ACS Earth Space Chem. 4, 515–525.
Wu, Y., Guo, J., Jiang, D., Zhou, P., Lan, Y., Zhou, L., 2012. Heterogeneous photocatalytic degradation of methyl orange in schwertmannite/oxalate suspension under UV irradiation. Environ. Sci. Pollut. Res. Int. 19, 2313–2320.
Xu, H., Allard, B., Grimvall, A., 1988. Influence of pH and organic substance on the adsorption of As(V) on geologic materials. Water Air Soil Pollut. 40, 293–305.
Xu, J., Li, J., Wu, F., Zhang, Y., 2014. Rapid photooxidation of As(III) through surface complexation with nascent colloidal ferric hydroxide. Environ. Sci. Technol. 48, 272–278.
Yang, X., Liu, L., Zhang, M., Tan, W., Qiu, G., Zheng, L., 2019. Improved removal capacity of magnetite for Cr(VI) by electrochemical reduction. J. Hazard. Mater. 374, 26–34.
Yu, R.X., Zhao, J.H., Zhao, Z.W., Cui, F.Y., 2020. Copper substituted zinc ferrite with abundant oxygen vacancies for enhanced ciprofloxacin degradation via peroxymonosulfate activation. J. Hazard. Mater. 390, 121998.
Yu, Y., Zhu, Y., Gao, Z., Gammons, C.H., Li, D., 2007. Rates of arsenopyrite oxidation by oxygen and Fe(III) at pH 1.8−12.6 and 15−45 ℃. Environ. Sci. Technol. 41, 6460–6464.
Yunmei, Y., Yongxuan, Z., Williams-Jones, A.E., Zhenmin, G., Dexian, L., 2004. A kinetic study of the oxidation of arsenopyrite in acidic solutions: implications for the environment. Appl. Geochem. 19, 435–444.
Zhang, J., Li, Y., Li, W., Zhou, L., Lan, Y., Guo, J., 2019. The synergistic trigger of the reductive dissolution of schwertmannite-As(III) and the release of arsenic from citric acid and UV irradiation. Chem. Geol. 520, 11–20.
Zhang, P., Yuan, S., 2017. Production of hydroxyl radicals from abiotic oxidation of pyrite by oxygen under circumneutral conditions in the presence of low-molecular-weight organic acids. Geochim. Cosmochim. Acta 218, 153–166.
Zhang, P., Yuan, S., Liao, P., 2016a. Mechanisms of hydroxyl radical production from abiotic oxidation of pyrite under acidic conditions. Geochim. Cosmochim. Acta 172, 444–457.
Zhang, S.L., Jia, S.Y., Yu, B., Liu, Y., Wu, S.H., Han, X., 2016b. Sulfidization of As(V)-containing schwertmannite and its impact on arsenic mobilization. Chem. Geol. 420, 270–279.
Zhang, T., Liu, L., Tan, W., Suib, S.L., Qiu, G., Liu, F., 2018a. Photochemical formation and transformation of birnessite: Effects of cations on micromorphology and crystal structure. Environ. Sci. Technol. 52, 6864–6871.
Zhang, W., Zhang, F.S., Liu, C.H., Li, J., Zheng, T., Ma, J., Wang, L., Jiang, J., Zhai, X.D., 2018b. Enhanced removal of arsenite and arsenate by a multifunctional Fe-Ti-Mn composite oxide: photooxidation, oxidation and adsorption. Water Res 147, 264–275.
Zheng, K., Li, H., Wang, S., Feng, X., Wang, L., Liu, Q., 2020. Arsenopyrite weathering in sodium chloride solution: Arsenic geochemical evolution and environmental effects. J. Hazard. Mater. 392, 122502.
Zhou, D., Wu, Y., Feng, X., Chen, Y., Wang, Z., Tao, T., Wei, D., 2014. Photodegradation of hexabromocyclododecane (HBCD) by Fe(III) complexes/H_2O_2 under simulated sunlight. Environ. Sci. Pollut. Res. 21, 6228–6233.